www.sciencemag.org/cgi/content/full/science.aaa7484/DC1

Supplementary Material for

Natural light-gated anion channels: A family of microbial rhodopsins for advanced optogenetics

Elena G. Govorunova, Oleg A. Sineshchekov, Roger Janz, Xiaoqin Liu, John L. Spudich*

*Corresponding author. E-mail: john.l.spudich@uth.tmc.edu

Published 25 June 2015 on *Science* Express
DOI: 10.1126/science.aaa7484

This PDF file includes:

Materials and Methods

Molecular biology

DNA polynucleotides encoding 7TM domains of *G. theta* opsins (295, 291 and 288 amino acid residues, corresponding to the JGI protein models 111593, 146828 and 161302, respectively) optimized for human codon usage were synthesized (Genewiz, South Plainfield, NJ) and cloned into the mammalian expression vector pcDNA3.1 (Life Technologies, Grand Island, NY) in frame with an EYFP tag. The sequence information encoding the functional constructs 111593 (*Gt*ACR1) and 146828 (*Gt*ACR2) were deposited in GenBank (accession numbers KP171708 and KP171709, respectively). The polynucleotides encoding the slow Chloc mutant and SwiChR$_{CT}$ mutant were synthesized (Genewiz) according to (*14*) and (*15*), respectively. The gene encoding archaerhodopsin-3 (Arch) was kindly provided by Dr. Edward S. Boyden (Massachusetts Institute of Technology, Boston, MA).

HEK293 recording

HEK293 (human embryonic kidney) cells were transfected using the ScreenFectA transfection reagent (Waco Chemicals USA, Richmond, VA). All-*trans*-retinal (Sigma) was added as a stock solution in ethanol at the final concentration of 5 μM. Measurements were performed 48-72 h after transfection with an Axopatch 200B amplifier (Molecular Devices, Union City, CA). The signals were digitized with a Digidata 1440A using pClamp 10 software (both from Molecular Devices). Patch pipettes with resistances of 2-5 MΩ were fabricated from borosilicate glass. The composition of solutions is shown in table S1. A 4 M salt bridge was used in all experiments. All *IE* dependencies were corrected for liquid junction potentials calculated using the ClampEx built-in LJP calculator (table S1). Continuous light pulses were provided by a Polychrome IV light source (T.I.L.L. Photonics GMBH, Grafelfing, Germany) in combination with a mechanical shutter (Uniblitz Model LS6, Vincent Associates, Rochester, NY; half-opening time 0.5 ms). The light intensity was attenuated with the built-in Polychrome system or with neutral density filters. Maximal quantum density at the focal plane of the 40x objective lens was 8.5 mW/mm^2. All measurements were carried out at room temperature (25° C). In experiments aimed to test cation permeability E_{rev} shifts were calculated by subtraction of the reference value measured at 150 mM NMG^+ in the bath from the values measured at 150 mM Na^+ (pH 5.4), 150 mM Na^+ (pH 7.4), 150 mM K^+ (pH 7.4) or 75 mM Ca^{2+} (pH 7.4). The Cl^- concentration in the bath was 155.6 mM with all cations. In tests of anion permeability E_{rev} shifts were calculated by subtraction of the reference value measured at 150 mM Asp^- from the value measured at 75 mM SO_4^{2-} or 150 mM of F^-, Br^-, I^- or NO_3^-. The Na^+ concentration in the bath was 150 mM with all anions except F^- (see table S1).

Stationary noise analysis was performed as described in detail in (*17*). Briefly, current traces were recorded at -60 mV in the dark and during a 48-s light pulse of intensity eliciting a half-maximal response. Power spectral densities were calculated using pClamp software. The difference (light minus dark spectrum) was fit between 0.3 Hz and 1 kHz with a single Lorentzian function using Origin 7 software (OriginLab Corporation, Northampton, MA) to determine the zero frequency asymptote and the

corner frequency. The unitary conductance was calculated from the parameters of this function and the amplitude of the whole-cell channel current, E_h and E_{rev}.

Fluorescence measurements

EYFP fluorescence was measured 48-72 h after transfection using a Nikon Eclipse Ti-U microscope equipped with a CoolSnap HQ2 CCD camera (Photometrics, Tucson, AZ). An X-Cite 120Q light source (EXFO, Mississauga, Ontario) was used for excitation, and fluorescence was detected using a Nikon B-2E/C filter set. All images were taken with the same acquisition parameters and analyzed with the ImageJ1.42q software.

Neuronal recording

For neuronal expression the *Gt*ACR2-EYFP construct was transferred to the pFUGW lentivirus vector provided by Dr. Carlos Lois (MIT, Boston, MA). The lentivirus was produced by triple transfection of HEK293FT cells (Invitrogen) with the envelope plasmid pCMV-VSVG, the packaging plasmid pΔ8.9 (both from Dr. Lois) and the pFUGW-*Gt*ACR2-EYFP plasmid using Lipofectamine 2000 (Invitrogen). Hippocampi of E18 Sprague Dawley rats were obtained as part of a kit from BrainBits (Springfield, IL), and primary neuronal cultures were prepared using the protocol provided by the company. Cells were cultured in NbActiv4 medium on poly-lysine coated coverslips and supplemented with 0.4 μM all-trans retinal (final concentration, in addition to retinyl acetate present in the medium). Patch-clamp measurements were carried out 10 to 19 days after transfection. The same photoexcitation source and measuring setup was used as described above for HEK cells. Correction for liquid junction potentials (table S2) was made as described for HEK cells. Spiking was measured in the current clamp mode. The composition of solutions is shown in table S2. All measurements were carried out at room temperature (25° C).

Analysis of neuronal morphology

Cultured hippocampal neurons were fixed in 4% paraformaldehyde in PBS after 8 days in culture (expressing *Gt*ACR2 for 7 days), washed 1 time in PBS, permeabilized with solution A (1% goat serum and 0.3% Triton X-100 in PBS), blocked with 5% goat serum in PBS, and then simultaneously incubated with rabbit anti-GFP antibody (Abcam, 1:1000) and mouse anti-SV2 antibody (Developmental Studies Hybridoma Bank, University of Iowa, 1:200) at 4°C overnight, treated with Alexa Fluor 488-conjugated goat anti-rabbit IgG and Alexa Fluor 568-conjugated goat anti-mouse IgG at room temperature for 30 minutes, washed with PBS, mounted with VectaShield mounting medium (Vector Laboratories, Burlingame, CA), and viewed under a laser scanning microscope (LSM 510 META, Carl Zeiss, Germany). Images were obtained with Zen lite software. Images of randomly selected neurons where used to quantify numbers of primary dendrites and synapse numbers. Primary dendrites where identified as originating from the soma and crossing a radius of 50 μm from the center of the soma. Synapse numbers where determined by analyzing SV2 stained images using ImageJ. Synaptic terminals where defined as spherical SV2 immunopositive particles of 0.06–0.23 μm^3 based on data from (*26*). Analysis was performed in a circle of 50 μm diameter around the center of the soma.

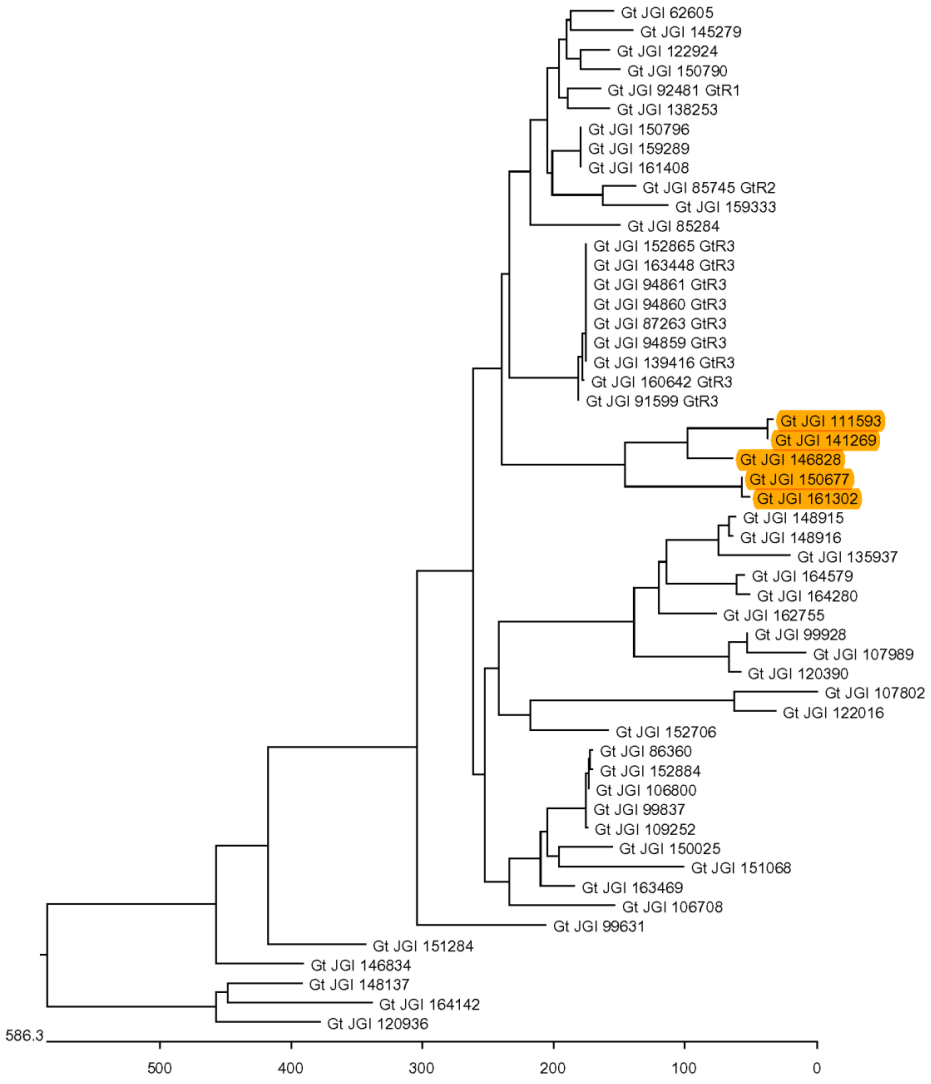

Fig. S1: Phylogenetic tree of *G. theta* protein models

The models homologous to microbial rhodopsins were selected among those predicted by the Joint Genome Institute (JGI) sequencing project (http://genome.jgi.doe.gov/Guith1/Guith1.home.html) and aligned using ClustalW. The tree was constructed using the neighbor-joining method. *Gt*R1, *Gt*R2 and *Gt*R3 are proteins identified previously. Eight models lack the conserved Lys residue in the seventh transmembrane helix that covalently links to retinal in known rhodopsins, and should therefore be considered opsin-related proteins.

The models that show the highest homology to chlorophyte ChRs are highlighted. Out of five members in this cluster, the models 111593 and 141269 differ only in a 7 residue-stretch in the middle of the sequence, and the models 161302 and 150677 differ only in the length of their C-termini. Therefore, we limited our analysis to the models 111593, 146828 and 161302. In addition to 7TM domains, these *G. theta* proteins contain long (~150 amino acid residues) C-terminal domains, as is also typical of chlorophyte ChRs.

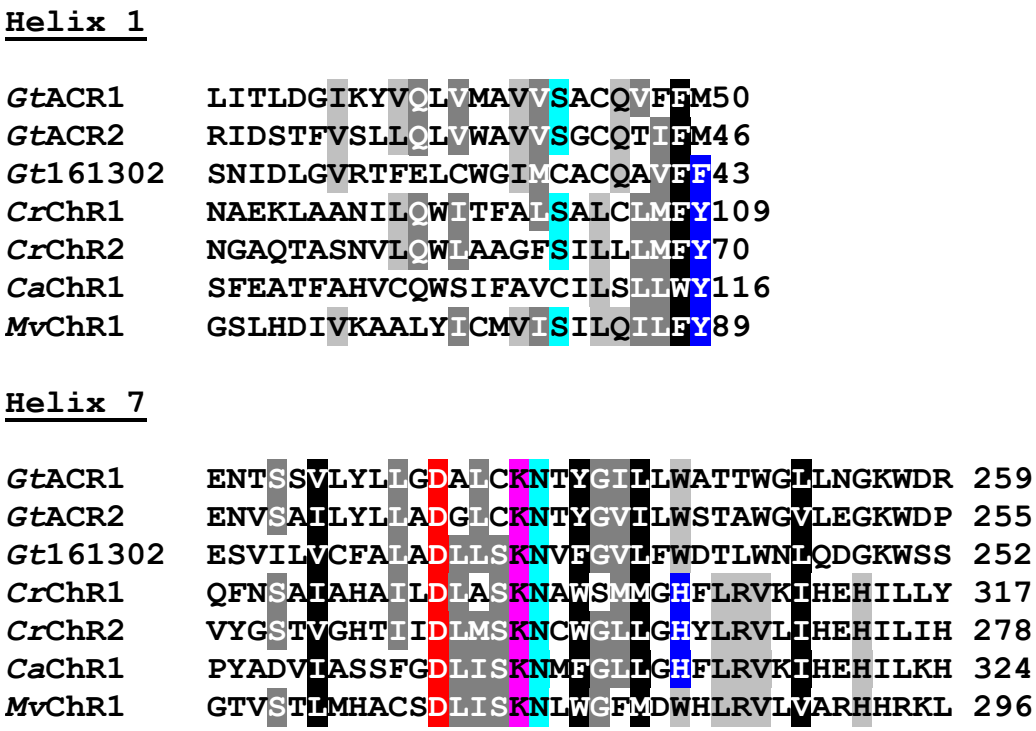

Fig. S2: ClustalW alignments of transmembrane helices 1 and 7

Abbreviated organism names are: *Gt, Guillardia theta*; *Cr, Chlamydomonas reinhardtii*; *Ca*, *Chlamydomonas augustae; Mv*, *Mesostigma viride.* The last residue numbers are shown on the right. The residues corresponding to Ser-102 (63) (*Cr*ChR1/*Cr*ChR2 numbering) in helix 1 and Asn-297 (258) in helix 7 that together with Glu-129 (90) form the central gate in the crystallized *Cr*ChR1/*Cr*ChR2 chimera (*27*) are conserved in the two functional *G. theta* ACRs (highlighted cyan). However, the residues that form the inner gate in the chimera, Tyr-109 (70), His-173 (134) and His-304 (265), are not conserved in the two functional ACRs (the Tyr and one of the His residues are highlighted blue above and the second His residue highlighted blue in Fig. 1C in the main text).

A conspicuous feature of ACRs is a non-carboxylic amino acid residue in the position of the proton acceptor Asp85 in bacteriorhodopsin, where nearly all cation-selective ChRs contain a Glu residue (highlighted red in Fig. 1C in the main text). A non-ionizable residue at the corresponding position is also typical of chloride-pumping rhodopsins from haloarchaea and marine flavobacteria, where the residue forms part of the chloride binding site in the unphotolyzed state as shown for haloarchaeal halorhodopsin (*28*).

The mechanism of anion conduction in ACRs appears to be different from that of the Cl^--conducting ChR mutants, as might be expected from their large difference in sequence. ACRs contain a Glu residue corresponding to Glu90 of the cation selectivity filter of *Cr*ChR2 (Fig. 1B in the main text) (*22, 29*). To confer Cl^- permeability to this cation-conducting channel, Glu90 required replacement with an uncharged (Ser (*15*)) or cationic (Lys or Arg (*14*)) residue. However, the presence of the Glu90 homolog in ACRs shows it is not a barrier to anion permeation in the anion channels unlike in the cation channels.

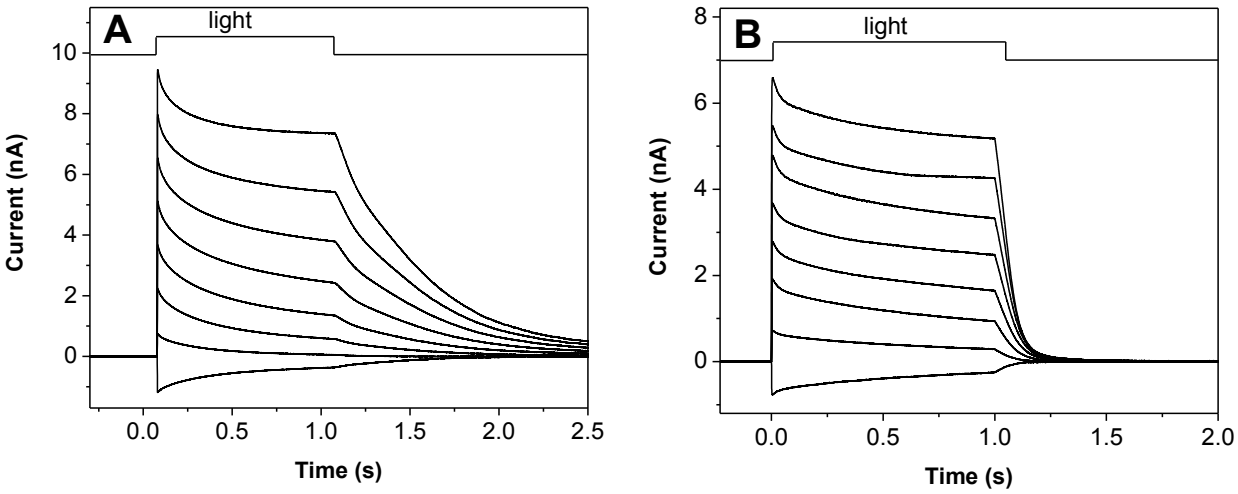

Fig. S3: Photocurrents generated by *Gt*ACR1 (A) and *Gt*ACR2 (B) in HEK293 cells with low Cl^- concentration in the pipette and high Cl^- concentration in the bath

The membrane potentials were changed in 20-mV steps from -80 mV at the amplifier output (bottom to top).

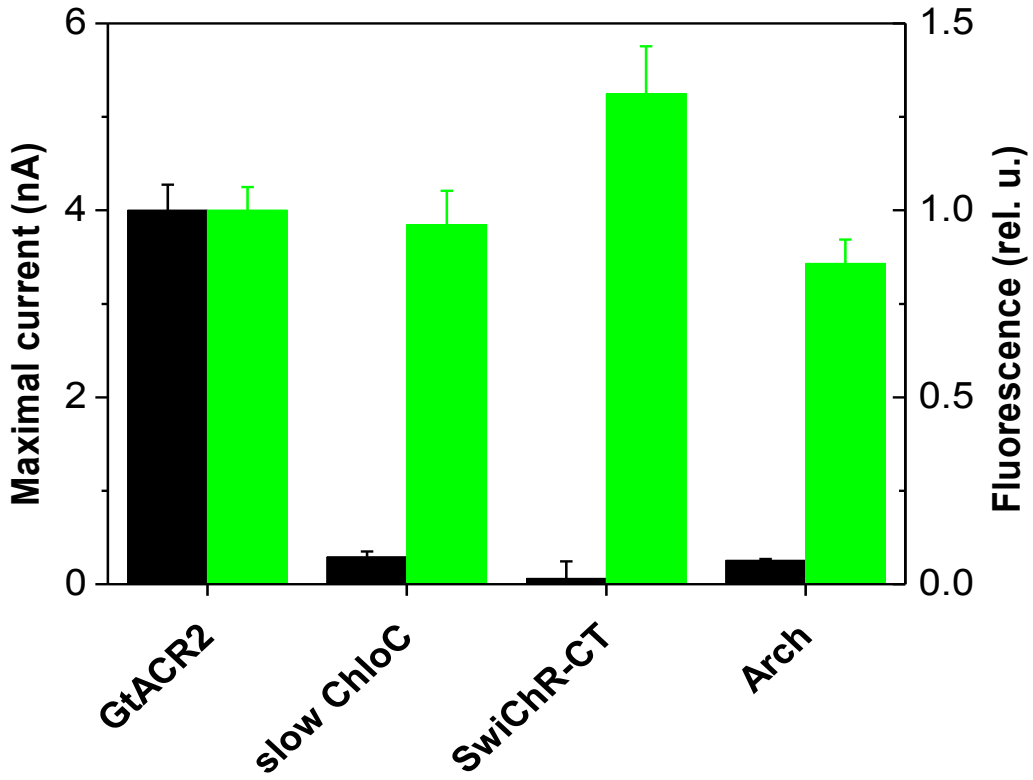

Fig. S4: Maximal photocurrents (black bars, left axis) and relative EYFP tag fluorescence (green bars, right axis) of hyperpolarizing optogenetic tools

The data are mean values ± SEM (n = 10-20 cells) with fluorescence normalized to the values obtained for *Gt*ACR2.

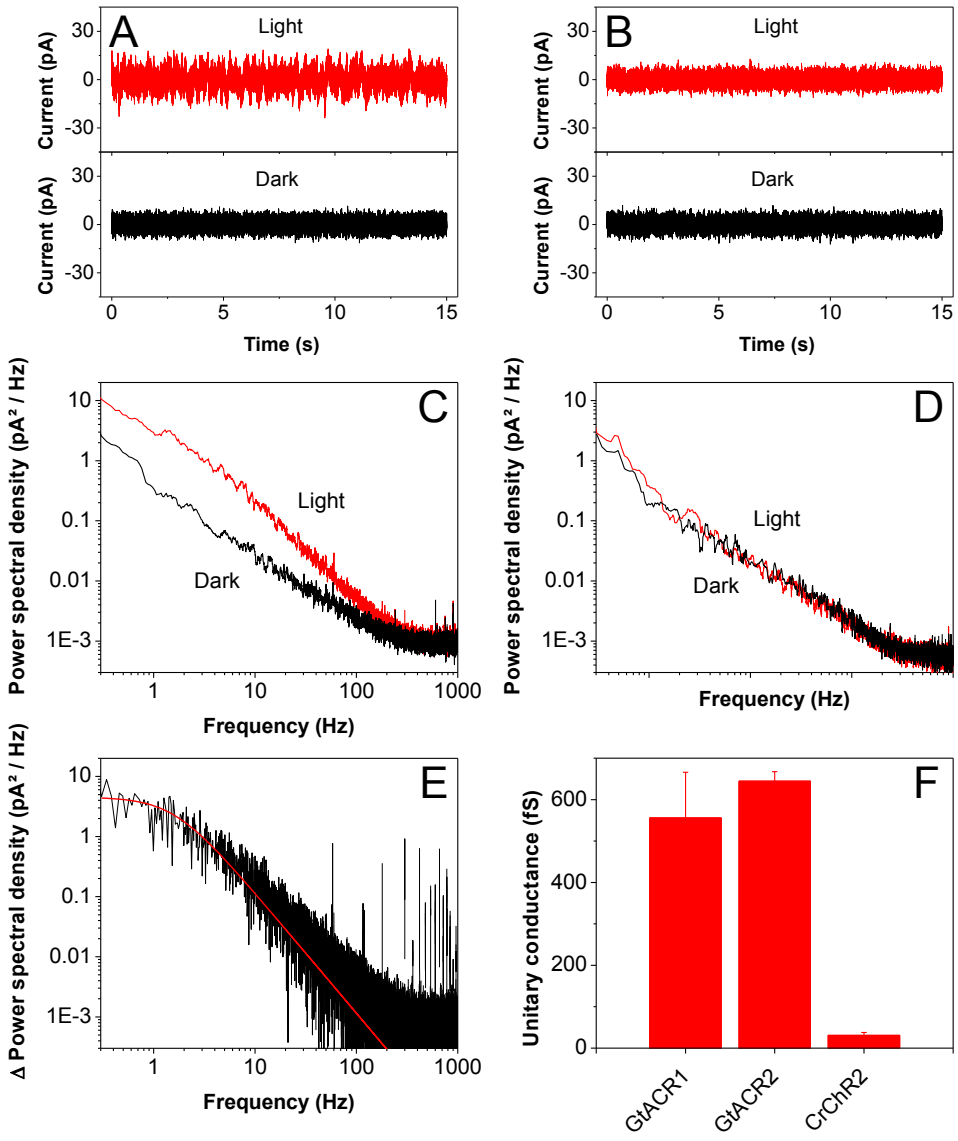

Fig. S5: Stationary analysis of current noise generated by ACRs and slow ChloC

(**A** and **B**) Representative noise traces recorded in the dark and under illumination at the light intensity eliciting half-maximal currents from HEK293 cells transfected with *Gt*ACR1 (A) or slow ChloC (B). (**C** and **D**) Representative power spectra of the current noise recorded in the dark and under illumination for *Gt*ACR1 (C) and slow ChloC (D), as shown in A and B, respectively. The spectra were smoothed by adjacent averaging for presentation purposes. For slow ChloC, no difference was observed between the dark and light spectra, so its unitary conductance could not be determined. (**E**) The light minus dark difference spectrum for *Gt*ACR1 prior to smoothing (black line) and its computer approximation with a Lorentzian function (red line). Analysis of *Gt*ACR2-generated noise was carried out in a similar manner and is not shown. (**F**) The unitary conductance of ACRs calculated from the parameters of the Lorentzian fits in this study (mean values ± SEM; n = 8-11) and of wild-type *Cr*ChR2 assayed under the same conditions from (*17*).

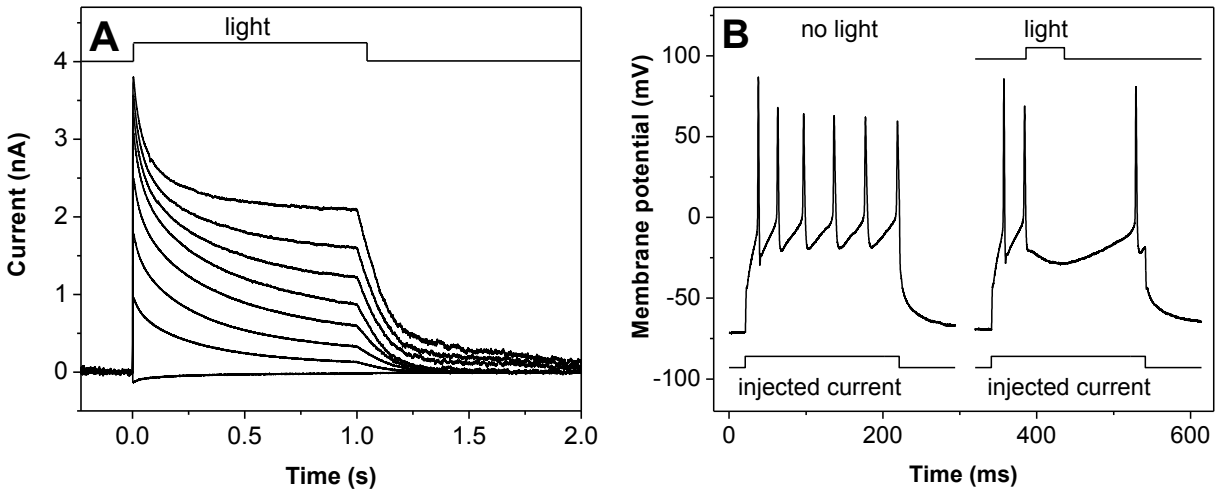

Fig. S6: *Gt*ACR2 function in cultured pyramidal neurons

(**A**) Photocurrents generated by *Gt*ACR2 in cultured pyramidal neurons at low Cl^- concentration in the pipette and high Cl^- concentration in the bath. The membrane potentials were changed in 20-mV steps from -80 mV at the amplifier output (bottom to top). (**B**) Representative traces of spiking of a *Gt*ACR2-transfected neuron in response to a prolonged injection of a depolarizing current in the dark (left) and its silencing by a shorter illumination pulse (right). The injected current was 300 pA, the light intensity was 0.026 mW/mm^2.

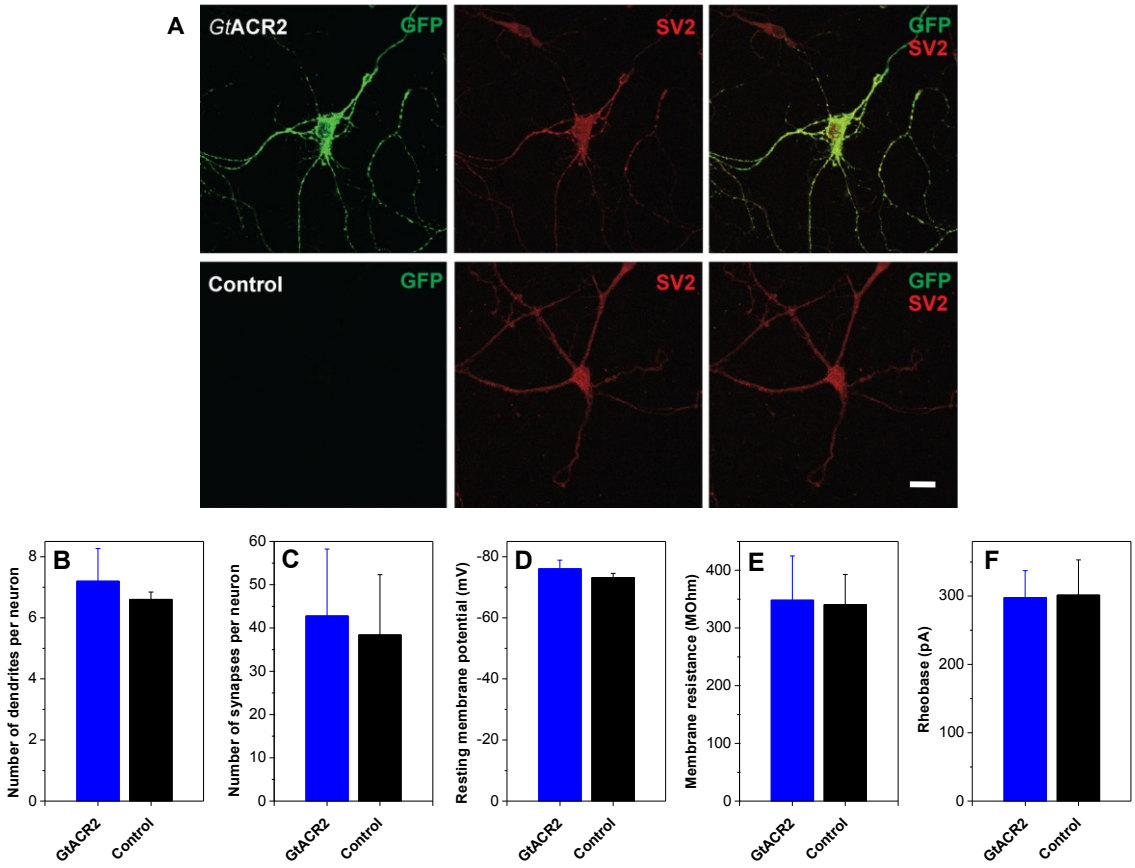

Fig. S7: Expression of *Gt*ACR2 does not affect morphology and electrical parameters of cultured neurons

(**A**) Representative images of *Gt*ACR2-expressing neurons (top row) demonstrate normal morphology when compared with control non-transfected neurons (bottom row). The neurons were infected with lentivirus one day after plating, fixed after 8 days in culture (7 days after infection) and labeled with antibodies against GFP (to label tagged *Gt*ACR2, green) and SV2 (a synaptic marker, red). Scale bar 20 µm. (**B**) The number of primary dendrites per neuron at a 50 µm radius around the center of the soma. (**C**) The number of synapses per neuron in a 50 µm circle around the center of the soma (**D**) The resting potential of neurons. (**E**) The membrane resistance of neurons. (**F**) Rheobase of ramp-evoked (1000 pA, 1 s) spiking in the dark. All data in panels (B-F) are mean values ± SEM (n = 5-7 cells). No statistically significant difference was detected between transfected and control non-transfected neurons (unpaired *t* test, two tailed).

Table S1: Composition of pipette and bath solutions and liquid junction potentials in experiments with HEK293 cells

Abbreviations: Asp, aspartate; EGTA, ethylene glycol tetraacetic acid; HEPES, 4-(2-hydroxyethyl)-1-piperazineethanesulfonic acid; LJP, liquid junction potential; NMG, N-Methyl-D-glucamine. All concentrations are in mM.

	NaCl	KCl	$CaCl_2$	$MgCl_2$	Na_2EGTA	HEPES	NMG	Glucose	NaAsp	NaF	NaBr	NaI	$NaNO_3$	Na_2SO_4	HCl	LJP pip. stand	LJP pip. Asp
Pipette standard	—	126	0.5	2	5	25	12.2	—	—	—	—	—	—	—	—	—	—
Pipette Asp	—	—	0.5	2	5	25	12.2	—	126	—	—	—	—	—	—	—	—
Bath standard	150	—	1.8	1	—	10	4.6	5	—	—	—	—	—	—	—	4.7	12.9
Bath Asp	—	—	1.8	1	—	10	4.6	5	150	—	—	—	—	—	—	-7	—
Bath pH 5.4	150	—	1.8	1	—	10	—	5	—	—	—	—	—	—	—	4.7	—
Bath K	—	150	1.8	1	—	10	4.6	5	—	—	—	—	—	—	—	0.3	—
Bath Ca	—	—	75	1	—	10	4.6	5	—	—	—	—	—	—	—	8.4	—
Bath NMG	1.5	—	1.8	1	—	10	148.5	5	—	—	—	—	—	—	148.5	10.7	—
Bath F	5.6	—	—	—	—	10	4.6	5	—	150	—	—	—	—	—	13.8	—
Bath Br	—	—	1.8	1	—	10	4.6	5	—	—	150	—	—	—	—	4.5	—
Bath I	—	—	1.8	1	—	10	4.6	5	—	—	—	150	—	—	—	4.3	—
Bath NO_3	—	—	1.8	1	—	10	4.6	5	—	—	—	—	150	—	—	3.3	—
Bath SO_4	—	—	1.8	1	—	10	4.6	5	—	—	—	—	—	75	—	-2.6	—

Table S2: Composition of pipette and bath solutions and liquid junction potentials in experiments with neurons

Abbreviations: HEPES, 4-(2-hydroxyethyl)-1-piperazineethanesulfonic acid; LJP, liquid junction potential; NMDG, N-Methyl-D-glucamine. All concentrations are in mM.

	K_2SO_4	KCl	NaCl	$CaCl_2$	$MgCl_2$	HEPES	Glucose	LJP
Pipette	67.5	—	—	—	2	—	—	—
Bath Tyrode	—	2	125	3	1	25	30	11.3

References

1. J. L. Spudich, O. A. Sineshchekov, E. G. Govorunova, Mechanism divergence in microbial rhodopsins. *Biochim. Biophys. Acta* **1837**, 546–552 (2014). Medline doi:10.1016/j.bbabio.2013.06.006

2. O. P. Ernst, D. T. Lodowski, M. Elstner, P. Hegemann, L. S. Brown, H. Kandori, Microbial and animal rhodopsins: Structures, functions, and molecular mechanisms. *Chem. Rev.* **114**, 126–163 (2014). Medline doi:10.1021/cr4003769

3. K. Deisseroth, Optogenetics. *Nat. Methods* **8**, 26–29 (2011). Medline doi:10.1038/nmeth.f.324

4. B. Y. Chow, E. S. Boyden, Optogenetics and translational medicine. *Sci. Transl. Med.* **5**, 177ps5 (2013). Medline doi:10.1126/scitranslmed.3003101

5. J. Y. Lin, P. M. Knutsen, A. Muller, D. Kleinfeld, R. Y. Tsien, ReaChR: A red-shifted variant of channelrhodopsin enables deep transcranial optogenetic excitation. *Nat. Neurosci.* **16**, 1499–1508 (2013). Medline doi:10.1038/nn.3502

6. O. A. Sineshchekov, K.-H. Jung, J. L. Spudich, Two rhodopsins mediate phototaxis to low- and high-intensity light in *Chlamydomonas reinhardtii*. *Proc. Natl. Acad. Sci. U.S.A.* **99**, 8689–8694 (2002). Medline doi:10.1073/pnas.122243399

7. G. Nagel, D. Ollig, M. Fuhrmann, S. Kateriya, A. M. Musti, E. Bamberg, P. Hegemann, Channelrhodopsin-1: A light-gated proton channel in green algae. *Science* **296**, 2395–2398 (2002). Medline doi:10.1126/science.1072068

8. G. Nagel, T. Szellas, W. Huhn, S. Kateriya, N. Adeishvili, P. Berthold, D. Ollig, P. Hegemann, E. Bamberg, Channelrhodopsin-2, a directly light-gated cation-selective membrane channel. *Proc. Natl. Acad. Sci. U.S.A.* **100**, 13940–13945 (2003). Medline doi:10.1073/pnas.1936192100

9. F. Zhang, L. P. Wang, M. Brauner, J. F. Liewald, K. Kay, N. Watzke, P. G. Wood, E. Bamberg, G. Nagel, A. Gottschalk, K. Deisseroth, Multimodal fast optical interrogation of neural circuitry. *Nature* **446**, 633–639 (2007). Medline doi:10.1038/nature05744

10. X. Han, E. S. Boyden, Multiple-color optical activation, silencing, and desynchronization of neural activity, with single-spike temporal resolution. *PLOS ONE* **2**, e299 (2007). Medline doi:10.1371/journal.pone.0000299

11. V. Gradinaru, K. R. Thompson, K. Deisseroth, eNpHR: A *Natronomonas* halorhodopsin enhanced for optogenetic applications. *Brain Cell Biol.* **36**, 129–139 (2008). Medline doi:10.1007/s11068-008-9027-6

12. B. Y. Chow, X. Han, A. S. Dobry, X. Qian, A. S. Chuong, M. Li, M. A. Henninger, G. M. Belfort, Y. Lin, P. E. Monahan, E. S. Boyden, High-performance genetically targetable optical neural silencing by light-driven proton pumps. *Nature* **463**, 98–102 (2010). Medline doi:10.1038/nature08652

13. A. S. Chuong, M. L. Miri, V. Busskamp, G. A. Matthews, L. C. Acker, A. T. Sørensen, A. Young, N. C. Klapoetke, M. A. Henninger, S. B. Kodandaramaiah, M. Ogawa, S. B. Ramanlal, R. C. Bandler, B. D. Allen, C. R. Forest, B. Y. Chow, X. Han, Y. Lin, K. M. Tye, B. Roska, J. A. Cardin, E. S. Boyden, Noninvasive optical inhibition with a red-shifted microbial rhodopsin. *Nat. Neurosci.* **17**, 1123–1129 (2014). Medline doi:10.1038/nn.3752

14. J. Wietek, J. S. Wiegert, N. Adeishvili, F. Schneider, H. Watanabe, S. P. Tsunoda, A. Vogt, M. Elstner, T. G. Oertner, P. Hegemann, Conversion of channelrhodopsin into a light-gated chloride channel. *Science* **344**, 409–412 (2014). Medline doi:10.1126/science.1249375

15. A. Berndt, S. Y. Lee, C. Ramakrishnan, K. Deisseroth, Structure-guided transformation of channelrhodopsin into a light-activated chloride channel. *Science* **344**, 420–424 (2014). Medline doi:10.1126/science.1252367

16. F. Zhang, J. Vierock, O. Yizhar, L. E. Fenno, S. Tsunoda, A. Kianianmomeni, M. Prigge, A. Berndt, J. Cushman, J. Polle, J. Magnuson, P. Hegemann, K. Deisseroth, The microbial opsin family of optogenetic tools. *Cell* **147**, 1446–1457 (2011). Medline doi:10.1016/j.cell.2011.12.004

17. E. G. Govorunova, O. A. Sineshchekov, H. Li, R. Janz, J. L. Spudich, Characterization of a highly efficient blue-shifted channelrhodopsin from the marine alga *Platymonas*

subcordiformis. *J. Biol. Chem.* **288**, 29911–29922 (2013). Medline doi:10.1074/jbc.M113.505495

18. N. C. Klapoetke, Y. Murata, S. S. Kim, S. R. Pulver, A. Birdsey-Benson, Y. K. Cho, T. K. Morimoto, A. S. Chuong, E. J. Carpenter, Z. Tian, J. Wang, Y. Xie, Z. Yan, Y. Zhang, B. Y. Chow, B. Surek, M. Melkonian, V. Jayaraman, M. Constantine-Paton, G. K. Wong, E. S. Boyden, Independent optical excitation of distinct neural populations. *Nat. Methods* **11**, 338–346 (2014). Medline doi:10.1038/nmeth.2836

19. O. A. Sineshchekov, E. G. Govorunova, K. H. Jung, S. Zauner, U. G. Maier, J. L. Spudich, Rhodopsin-mediated photoreception in cryptophyte flagellates. *Biophys. J.* **89**, 4310–4319 (2005). Medline doi:10.1529/biophysj.105.070920

20. V. Gradinaru, F. Zhang, C. Ramakrishnan, J. Mattis, R. Prakash, I. Diester, I. Goshen, K. R. Thompson, K. Deisseroth, Molecular and cellular approaches for diversifying and extending optogenetics. *Cell* **141**, 154–165 (2010). Medline doi:10.1016/j.cell.2010.02.037

21. B. A. Curtis, G. Tanifuji, F. Burki, A. Gruber, M. Irimia, S. Maruyama, M. C. Arias, S. G. Ball, G. H. Gile, Y. Hirakawa, J. F. Hopkins, A. Kuo, S. A. Rensing, J. Schmutz, A. Symeonidi, M. Elias, R. J. Eveleigh, E. K. Herman, M. J. Klute, T. Nakayama, M. Oborník, A. Reyes-Prieto, E. V. Armbrust, S. J. Aves, R. G. Beiko, P. Coutinho, J. B. Dacks, D. G. Durnford, N. M. Fast, B. R. Green, C. J. Grisdale, F. Hempel, B. Henrissat, M. P. Höppner, K. Ishida, E. Kim, L. Kořený, P. G. Kroth, Y. Liu, S. B. Malik, U. G. Maier, D. McRose, T. Mock, J. A. Neilson, N. T. Onodera, A. M. Poole, E. J. Pritham, T. A. Richards, G. Rocap, S. W. Roy, C. Sarai, S. Schaack, S. Shirato, C. H. Slamovits, D. F. Spencer, S. Suzuki, A. Z. Worden, S. Zauner, K. Barry, C. Bell, A. K. Bharti, J. A. Crow, J. Grimwood, R. Kramer, E. Lindquist, S. Lucas, A. Salamov, G. I. McFadden, C. E. Lane, P. J. Keeling, M. W. Gray, I. V. Grigoriev, J. M. Archibald, Algal genomes reveal evolutionary mosaicism and the fate of nucleomorphs. *Nature* **492**, 59–65 (2012). Medline

22. D. Gradmann, A. Berndt, F. Schneider, P. Hegemann, Rectification of the channelrhodopsin early conductance. *Biophys. J.* **101**, 1057–1068 (2011). Medline doi:10.1016/j.bpj.2011.07.040

23. T. J. Jentsch, V. Stein, F. Weinreich, A. A. Zdebik, Molecular structure and physiological function of chloride channels. *Physiol. Rev.* **82**, 503–568 (2002). Medline

24. P. Bregestovski, T. Waseem, M. Mukhtarov, Genetically encoded optical sensors for monitoring of intracellular chloride and chloride-selective channel activity. *Front. Mol. Neurosci.* **2**, 15 (2009). Medline doi:10.3389/neuro.02.015.2009

25. K. Feldbauer, D. Zimmermann, V. Pintschovius, J. Spitz, C. Bamann, E. Bamberg, Channelrhodopsin-2 is a leaky proton pump. *Proc. Natl. Acad. Sci. U.S.A.* **106**, 12317–12322 (2009). Medline doi:10.1073/pnas.0905852106

26. T. Schikorski, C. F. Stevens, Quantitative ultrastructural analysis of hippocampal excitatory synapses. *J. Neurosci.* **17**, 5858–5867 (1997). Medline

27. H. E. Kato, F. Zhang, O. Yizhar, C. Ramakrishnan, T. Nishizawa, K. Hirata, J. Ito, Y. Aita, T. Tsukazaki, S. Hayashi, P. Hegemann, A. D. Maturana, R. Ishitani, K. Deisseroth, O. Nureki, Crystal structure of the channelrhodopsin light-gated cation channel. *Nature* **482**, 369–374 (2012). Medline doi:10.1038/nature10870

28. M. Kolbe, H. Besir, L. O. Essen, D. Oesterhelt, Structure of the light-driven chloride pump halorhodopsin at 1.8 A resolution. *Science* **288**, 1390–1396 (2000). Medline doi:10.1126/science.288.5470.1390

29. K. Ruffert, B. Himmel, D. Lall, C. Bamann, E. Bamberg, H. Betz, V. Eulenburg, Glutamate residue 90 in the predicted transmembrane domain 2 is crucial for cation flux through channelrhodopsin 2. *Biochem. Biophys. Res. Commun.* **410**, 737–743 (2011). Medline doi:10.1016/j.bbrc.2011.06.024